NEOPLASIA
www.neoplasia.com

Volume 10 Number 8 August 2008 pp. 745–756 745

Regulation of the Warburg Effect in Early-Passage Breast Cancer Cells[1,2]

Ian F. Robey*, Renu M. Stephen†, Kathy S. Brown*, Brenda K. Baggett*, Robert A. Gatenby‡,§ and Robert J. Gillies*,‡,¶

*Arizona Cancer Center, University of Arizona, Tucson, AZ, 85724 USA; †Department of Nutritional Sciences, University of Arizona, Tucson, AZ, 85724 USA; ‡Department of Radiology, University of Arizona, Tucson, AZ, 85724 USA; §Department of Applied Mathematics, University of Arizona, Tucson, AZ, 85724 USA; ¶Department of Biochemistry, University of Arizona, Tucson, AZ, 85724 USA

Abstract

Malignancy in cancer is associated with aerobic glycolysis (Warburg effect) evidenced by increased trapping of [^{18}F]deoxyglucose (FdG) in patients imaged by positron emission tomography (PET). [^{18}F]deoxyglucose uptake correlates with glucose transporter (GLUT-1) expression, which can be regulated by hypoxia-inducible factor 1 alpha (HIF-1α). We have previously reported in established breast lines that HIF-1α levels *in the presence of oxygen* leads to the Warburg effect. However, glycolysis and GLUT-1 can also be induced independent of HIF-1α by other factors, such as c-Myc and phosphorylated Akt (pAkt). This study investigates HIF-1α, c-Myc, pAkt, and aerobic glycolysis in low-passage breast cancer cells under the assumption that these represent the *in vivo* condition better than established lines. Similar to *in vivo* FdG-PET or primary breast cancers, rates of glycolysis were diverse, being higher in cells expressing both c-Myc and HIF-1α and lower in cell lines low or negative in both transcription factors. No correlations were observed between glycolytic rates and pAkt levels. Two of 12 cell lines formed xenografts in mice. Both were positive for HIF-1α and phosphorylated c-Myc, and only one was positive for pAkt. Glycolysis was affected by pharmacological regulation of c-Myc and HIF-1α. These findings suggest that c-Myc and/or HIF-1α activities are both involved in the regulation of glycolysis in breast cancers.

Neoplasia (2008) 10, 745–756

Introduction

Breast cancer is the most commonly diagnosed cancer among women in the United States [1]. Thus, accurate methods for staging and diagnosis would have significant clinical benefit. Whole-body noninvasive imaging of [^{18}F]deoxyglucose uptake using positron emission tomography (FdG-PET) is considered to be the most reliable technique for the evaluation and prognosis of breast cancer [2–6]. FdG-PET has been shown to accurately detect and differentiate malignant from normal tissues at sensitivities of greater than 90% in breast and other cancers [7–10]. Positron emission tomography imaging in breast cancer is especially precise in the detection of nodal or distant metastases [11–19]. However, the role of FdG-PET in the detection and diagnosis of primary breast cancer is not well established due to the limitations in detecting small-sized tumors with differentiated histologic types [14,18,20–22] and heterogeneous FdG uptake profiles [2,7,18,20–27].

Abbreviations: LPR, lactate production rate; GUR, glucose uptake rate; HIF-1α, hypoxia-inducible factor 1 alpha; SCID, severe combined immunodeficient; FdG, [^{18}F]deoxyglucose; TPA, 2-*O*-tetradecanoylphorbol-13-acetate

Address all correspondence to: Ian F. Robey, PhD, Arizona Cancer Center, 1656 E. Mabel, Tucson, AZ 85724. E-mail: robeyi@email.arizona.edu

[1]This work was funded by grants from the National Institutes of Health (RO1-CA77575 and RO1-CA77975-05) and Graduate Training in Physiology grant T32 HL007249-27. Primary breast tumor cells were supplied by the Arizona Cancer Center Cell Culture Shared Resource and the Arizona Cancer Center support grant (NIH-NCI 3P30 CA 2307). Immunohistochemical or histologic data generated by the Tissue Acquisition and Cellular/Molecular Analysis Shared Service Core was supported by the Arizona Cancer Center support grant, NIH CA023074.

[2]This article refers to a supplementary material, which is designated by Figure W1 and is available online at www.neoplasia.com.

Received 14 August 2007; Revised 30 April 2008; Accepted 1 May 2008

DOI 10.1593/neo.07724

A hallmark of malignant cancers is elevated uptake of glucose even under normal oxygen conditions, known as "aerobic glycolysis" or the Warburg effect [28]. Thus, the activity of glycolysis is elevated independent of oxygen and is thus distinguished from the Pasteur effect, which describes the elevation of glycolysis in response to hypoxia. For reasons not fully understood, cells with a Warburg effect continue to catabolize glucose at a high rate, even when mitochondrial oxidative pathways are available [29].

FdG-PET imaging does not differentiate between hypoxic (Pasteur effect) and aerobic (Warburg effect) glycolysis, but studies using combined 18-FdG and 18-F-misonidazole imaging have demonstrated that FdG avidity and hypoxia are not highly correlated *in vivo* [30,31]. Elevated aerobic glycolysis is a negative prognostic indicator and may endow tumors with invasive potential and resistance to radiation and chemotherapies [32,33]. FdG-PET imaging is used as a therapy response biomarker [34,35], and thus, increased knowledge regarding the regulation of deoxyglucose uptake is needed.

We have proposed that the aerobic glycolytic phenotype is established in premalignant lesions (e.g., ductal carcinoma *in situ*, DCIS), which grow toward ductal lumens where oxygen levels become limiting. In DCIS, the intervening basement membrane serves as a physical barrier preventing angiogenesis from relieving hypoxic stress, leading to cyclic and intermittent hypoxia in periluminal cells [36–39]. This microenvironmental stress promotes the selection of cells that exhibit a phenotype with constitutive up-regulation of glycolysis [32,40]. Explicit in our models is the concept that, because selection is based on phenotype and not genotype, multiple molecular mechanisms may be observed that would impact a common phenotype (e.g., aerobic glycolysis) [41]. One known mechanism is the stabilization of the hypoxia-inducible factor 1 alpha (HIF-1α), which will up-regulate genes necessary for maintaining tumor survival under stress, including angiogenic factors and glycolytic enzymes [42–44]. We have further proposed that, in metastases, the glycolytic phenotype persists due to increased production of glucose-derived acid, which potentiates invasiveness of cells into the extracellular matrix of the host tissue [32].

The molecular events leading to a glycolytic phenotype in breast cancer are not well known [45]. Oncogenic factors including c-Myc [46–48], Akt [49], and HIF-1α [50–54] have been implicated in regulating aerobic glycolysis. These factors share a common prevalence in many types of cancers, are typically associated with cellular response to stress, and demonstrate pleiotropic properties, including the capacity to induce transcription of glycolytic genes. Therefore, it is reasonable to hypothesize that evolving cells constitutively up-regulate one or more of these factors to establish the Warburg effect during carcinogenesis. Notable cross talk exists between these systems, viz, phosphorylated Akt (pAkt) can stimulate HIF-1α and HIF-1α can inhibit the transactivation activity of c-Myc [55].

We have previously shown that HIF-1α was responsible for the Warburg effect in established breast and renal cancer cell lines [52]. In the current work, we extend these analyses to a panel of low-passage breast cancer lines, with the assumption that these primary cells are more closely related to cells *in vivo*, compared to more established cell lines. This investigation cross-correlated the glucose uptake (GURs) and lactate production rates (LPRs) and the expression of glucose transporter, GLUT-1, with the expression of activated pAkt, c-Myc, and HIF-1α levels by immunoblot analysis and enzyme-linked immunosorbent assay (ELISA). The primary lines were characterized under atmospheric (160 mm Hg) oxygen. Notably, a wide range of glycolytic activities was observed across the cell lines, consistent with the variable levels of FdG uptake observed in patients. No correlations between pAkt and glucose consumption or LPRs were observed, whereas 10 of 12 cell lines showed significant correlations between glycolytic rates and phosphorylated c-Myc and HIF-1α levels, which may be interdependent. We investigated this further by treating cultured tumor cells with 2-*O*-tetradecanoylphorbol-13-acetate (TPA) to stimulate c-*myc* transactivation. Treatment up-regulated both phosphorylated c-Myc and nuclear HIF-1α expression and was accompanied by an increase in glycolysis. In addition, inhibition of HIF-1α activity with *S*-2-amino-3-[4′-*N*,*N*,-bis(2-chloroethyl)amino]phenyl propionic acid *N*-oxide dihydrochloride (PX-478) [56] caused a dose-dependent decrease in GURs. Thus, these data support the hypothesis that either HIF-1α or c-Myc can function to induce the Warburg effect in breast cancers.

Materials and Methods

Cells and Reagents

Cell lines were obtained from the Arizona Cancer Center tumor cell repository (Table 1). Tissue sources include surgically removed primary cancers, mostly pleural fluid efflusates and lymph node metastases, and one isolated from ascites. Tumors were placed in a sterile Petri dish and covered with M15 medium. M15 medium is composed of Leibovitz's L-15 medium containing glutamine, transferrin hydrocortisone, insulin, catalase, 2-mercaptoethanol, 10 mg/ml penicillin/streptomycin (Sigma, St. Louis, MO), and 5% FBS. Necrotic tissue, adherent connective tissue, fat, and blood clots were removed from the tumor, and the remaining tumor tissue was transferred to a fresh Petri dish containing medium. Tumor tissue was minced into 1- to 2-cm sections using a sterile, a #10 scalpel. Tumor samples were transferred to a conical tube, and medium was added. The supernatant containing single cells and small-cell clusters was collected and placed into a new conical tube. The remaining pellet was resuspended in medium and centrifuged at 1000 rpm for 5 minutes. The supernatant was discarded, and the pellet was resuspended in a collagenase solution (250 mg/100 ml). Tumor samples were incubated from 2 hours to overnight at 37°C, checking hourly for loosened clusters with individual rounded cells. After incubation, medium was added to the top of the tube and centrifuged at 1000 rpm for 5 minutes. The supernatant was removed, and the pellet was resuspended in fresh medium. The supernatant containing single cells and small-cell clusters was removed and placed into a new conical tube. Samples were incubated with disaggregating enzymes if large tumor sections existed. Tumor cells were qualitatively observed by optical microscopy. Debris and red blood cells were removed using BSA debris removal technique [57]. Tumor cells were seeded in tissue flasks and grown in a 37°C incubator at 5% CO_2.

Cells were maintained with weekly feedings involving the replacement of spent medium with new nutrient-rich growth medium. Cell lines growing in log phase (80% confluent) were subcultured in new flasks in lesser numbers to induce active growth phase. The remaining cells were kept frozen in liquid nitrogen. All cells have been cultured under 10 passages. Established cell lines, MDA-mb-231 and MDA-mb-435, were obtained from the American Type Culture Collection (Rockville, MD) and maintained in Dulbecco's modified Eagle's medium/F-12 supplemented with 10% FBS.

For tumor growth, 10^7 cells were suspended in 0.1 ml of Matrigel and were injected bilaterally into mammary fat pads of 6-week-old

Table 1. Low-Passage Breast Cancer Cell Lines from Arizona Cancer Center, Indicating Pathodiagnosis, Site of Collection, Age of Patient at Collection, Positive and Negative Markers, and Prior Treatments Before Collection.

Arizona Cancer Center Cell Culture Core Facility						
Established Breast Cell Line List						
ACC#	Pathology	Site	Age (years)	Positive Markers	Negative Markers	Treatment
732	Adenocarcinoma	Pleural fluid	35	neu, PR	ER; EGFR	VAC
812	Infiltrating ductal CA	Left breast (primary)	43	neu	ER, PR, EGFR	VAC then CMF
893	Infiltrating ductal CA	Right breast (primary)	57	neu, MAK-6	ER, PR, EGFR	None
1179	Adenocarcinoma	Pleural fluid	62	neu	ER, PR, EGFR	A, C, M, T
2087	Adenocarcinoma	Left pleural fluid	53	EGFR, ka4, MAK-6, 10.11	ER, PR, neu; vim	CMFVP, T
2150	Stage IIIB carcinoma	Right pleural fluid	47	neu, MAK-6	ER, PR, EGFR, ras	FAC, T, mito, velban
2648	Infiltrating ductal + lobular CA	Right pleural fluid	58	ER, PR, ka4, 10.11	neu, EGFR, vim	A, V, CMF/TP, velban, suramin/thiotepa
2715	Infiltrating ductal CA	Left pleural fluid	66	ka4, 10.11, MAK-6	ER, PR, EGFR, neu, vim	T, Megace, CMF, A
2925	Infiltrating ductal + lobular CA	Ascites	46		ER, PR, EGFR, neu	CMF, FAC, T, Mx, V
3133	Poorly differentiated adenocarcinoma + lobular CA	Pleural fluid	63	neu	ER, PR, EGFR	Surgery only
3171	Poorly differentiated metastatic carcinoma	Lymph node	42	S-100	ER, PR, EGFR, neu, CEA, vim	CAF
3199	Infiltrating ductal CA	Axillary nodes	58	EGFR	ER, PR, neu	CAF, T, Mx, V

CEA indicates carcinoembryonic antigen; *EGFR*, epidermal growth factor receptor; *ER/PR*, estrogen and progesterone receptor status of cell line; *ka4*, *10.11*, and *MAK-6* recognize cytokeratins 8, 14, 15, 16, 18, and 19; *neu*, HER-2/neu oncogene; *ras*, oncogene product; *S-100*, serum protein elevated in the blood of patients with metastatic disease; *vim*, vimentin.
Treatments: *A* indicates adriamycin; *C*, cytoxan; *CMF*, cyclophosphamide, methotrexate, and 5-fluorouracil combination therapy; *CMF/TP*, CMF with thymidine phosphorylase; *F*, 5-fluorouracil; *M*, methotrexate; *Megace*, megesterol acetate; *mito*, mitomycin C; *Mx*, mitoxantrone; *suramin/thiotepa*, cancer drugs; *T*, tamoxifen; *V*, vinblastine; *velban*, vinblastine.

female severe combined immunodeficient (SCID) mice at the Arizona Cancer Center Experimental Mouse Shared Service. Tumor formation was monitored and measured electronically on a weekly basis.

Glucose Uptake

Glucose-trapping experiments were carried out as previously described [52]. Briefly, cells growing in log phase were plated in 24-well plates and allowed to attach. Cultures were washed in glucose-free RPMI medium and treated with 4 μCi of [^{3}H]-2-deoxy-D-glucose in 5.56 mM D-(+)-glucose–supplemented medium for a 1-hour incubation period. Control experiments showed that [^{3}H]-2-deoxy-D-glucose uptake was linear over this period. Supernatant was sampled for liquid scintillation counting using a liquid scintillation counter (5000TD; Beckman Coulter, Inc., Brea, CA). Cells were washed and lysed with 0.1 N NaOH for 1 minute to generate extract samples for liquid scintillation counting. The remaining lysate was neutralized with 0.1 N HCl and assayed for protein concentration using Bradford reagent (Pierce, Rockford, IL). Glucose uptake rates were calculated as nmol/min per milligram protein.

Lactate Production Assay

Cells growing in 96-well plates were washed three times with glucose-free RPMI and treated with 10 mM D-(+)-glucose–supplemented, serum-free RPMI for 1 hour incubation at 37°C in a humidified 5% CO_2 atmosphere. Lactate levels were quantified using an enzymatically coupled lactic acid detection reagent (Sigma). Protein concentrations were obtained and measured as described previously. Lactate production rates were expressed as nmol/min per milligram protein.

Real-Time Quantitative Polymerase Chain Reaction

Total RNA was isolated from cell lines with a GenElute Mammalian Total RNA Miniprep Kit (Sigma) according to the manufacturer's instructions, followed by DNase treatment. Nucleic acid purity and concentration ($OD_{260/280}$) were measured on a μQuant universal microplate spectrophotometer (Bio-Tek Instruments, Inc., Winooski, VT). Reactions were carried out on a SmartCycler (Cephid, Foster City, CA) using a SYBR Green reverse transcription–polymerase chain reaction kit (Qiagen, Valencia, CA). Primers amplifying the human gene products were as follows: GLUT-1 (forward – TCAATGCTGATGATGAAC CTGCT, reverse – GGTGACACTTCACCCAC A TACA); and β-actin (forward – CCGCATCGTCACCAACTG, reverse – GGCACACGCAGC TCATTG) (Invitrogen, Carlsbad, CA). Data were normalized with the housekeeping gene, *β-actin*, as an internal control using the following formula: Relative gene expression = $2^{([\beta\text{-actin } Ct] - [\text{target gene } Ct])}$ [58].

Immunoblot Analysis and Immunohistochemistry

Cell extracts were processed with NE-PER Nuclear and Cytoplasmic Extraction Reagents (Pierce). Whole-cell lysates were prepared for measuring membrane-bound GLUT-1 using a cell-lysing reagent (Promega, Madison, WI). Extracts at equal concentrations (40 μg) were separated electrophoretically on an 11% polyacrylamide gel and transferred to Polyscreen PDVF blotting membrane (Perkin Elmer, Boston, MA). Immunoblot analysis techniques were carried out according to a protocol provided by Cell Signaling Technology (http://www.cellsignal.com/index.asp). Blots were probed overnight at 4°C with primary antibodies against human HIF-1α (1:250; Transduction Laboratories, Lexington, KY), phosphorylated c-Myc$^{Thr58/Ser62}$ (1:1000), total c-Myc (1:1000; Cell Signaling, Danvers, MA), pAkt^{Ser473} (1:1000), total Akt (1:1000; Cell Signaling Technology, Beverly, MA), HIF-2α (1:100, catalogue no. GTX28365; GeneTex, San Antonio, TX), GLUT-1 (1:100), actin (1:400), and nuclear lamin (1:200; Santa Cruz Biotechnology, Santa Cruz, CA). Membranes were counterprobed with HRP-conjugated antimouse, -goat, or -rabbit polyclonal IgG (1:10,000; Santa Cruz Biotechnology) secondary antibodies for 1 hour at room temperature. Blots were incubated in chemiluminescent substrate (Amersham Pharmacia, Uppsala, Sweden) for 1 minute and imaged using a VersArray 1300B cooled charge-coupled device camera (Roper Scientific, Duluth, GA) or exposed on BioMax film (Kodak, Rochester, NY). For presentation purposes, the qualitative images used in Figure 2 were selected from multiple blots carried out in separate experiments as representative results. Raw data are available in Figure W1.

For immunohistochemistry, the tumor sections were placed immediately in ice-cold 1% formalin containing a phosphatase-inhibiting reagent (Ventana Medical Systems, Tucson, AZ), dehydrated, paraffin-embedded, and stained by the Tissue Acquisition and Cellular Macromolecular Analysis Shares Service of the Arizona Cancer Center. A series of sequential 7-μm sections were cut from the center of fixed tumors, stained with eosin, and counterstained for antigens (pAkt and total Akt). Antibodies were be coupled to HRP and stained with diaminobenzidine (DAB). Images were digitized in RGB using a 1× objective on an inverted bright field microscope (Diaphot; Nikon, Melville, NY) coupled to a 12-Megapixel charge-coupled device (Photometrics, Tucson, AZ) with an 8-mm field of view, yielding a nominal resolution of 2.2 × 2.2 μm^2.

Enzyme-Linked Immunosorbent Assay

Semiquantitative levels of nuclear HIF-1α transactivation activity were measured by TransBinding HIF-1α Assay Kit (Panomics, Redwood City, CA) according to the manufacturer's instructions. C-Myc activity was measured similarly by TransAM Transcription Factor Assay Kit (Active Motif, Carlsbad, CA). Values were expressed as absorbance measurements (450 nm) normalized to protein concentrations after subtraction of negative control background absorbance.

Transcription Factor Induction and Inhibition

At 24 hours before treatment with TPA, cells seeded in 24-well assay plates were grown in serum-free RPMI. The medium was removed and replaced with RPMI containing 10% FBS and 15 nM TPA. Cells were allowed to incubate in normoxia for 2 hours with untreated controls. Cells were subsequently tested for supernatant lactate levels and harvested for protein extraction and immunoblot analysis experiments.

Anti–HIF-1α PX-478 was kindly donated by Garth Powis from the Arizona Cancer Center, Tucson, AZ. Toxicity thresholds were measured in both cell lines by crystal violet analysis (unpublished data). MDA-mb-231 cells were grown to 80% confluency then treated with nontoxic doses of PX-478 resuspended in growth medium. Cells were grown 24 hours under hypoxia (O_2 = 2%) at 37°C. Cultures were tested for GUR and harvested for protein extraction and immunoblot analysis experiments.

Statistics

All statistical calculations were determined using the analysis feature in GraphPad Prism version 4.03 for Windows (GraphPad Software, San Diego CA; http://www.graphpad.com). Linear regression was used to test whether the slope of the line deviated from the zero slope in data sets. Unpaired, two-tailed *t* tests were used to determine whether means were significantly different between the two data sets. Data set correlations were considered significant when $P < .05$.

Results

Breast Tumor Lines Exhibit Variable Rates of Glucose Uptake and Lactate Production under Normoxic Conditions

FdG-PET is generally equivocal in diagnosing and staging breast cancers because of its high variability [3,7,18,20–27]. To investigate the molecular basis of such variation, the glycolytic phenotypes of low-passage breast tumor lines were examined *in vitro* with glucose uptake, lactate production, and GLUT-1 mRNA transcript expression. Established metastatic breast cancer lines MDA-mb-231 and MDA-mb-435 were included in these studies as reference points for other published studies. The results from these experiments are summarized in Table 2.

Specific rates of glucose trapping were determined using [^{3}H]-2-deoxy-D-glucose (2dG) in RPMI medium. The mean uptake rate was 2.3 ± 0.4 nmol/min per milligram protein with a range of 0.6 to 5.6 nmol/min per milligram protein. Four of the 12 cell lines (ACC-3199, ACC-893, ACC-2638, and ACC-2087) exhibited uptake rates comparable to both MDA-mb-231 and MDA-mb-435, whereas four other cell lines (ACC-732, ACC-1179, ACC-3133, and ACC-2925) had significantly lower rates than MDA-mb-231 ($P < .05$). Cell lines ACC-2715 and ACC-3171 exhibited uptake rates significantly lower than MDA-mb-231 and MDA-mb-435, whereas cell lines ACC-812 and ACC-2150 consumed glucose at a significantly higher rate than the established lines ($P < .05$).

Although 2dG trapping is an effective kinetic evaluation of facilitative glucose transporter and hexokinase activities, it does not measure glucose metabolism. To verify that glucose uptake resulted in metabolism, LPRs were also determined under the same conditions. The mean LPR was 9.3 ± 1.3 nmol/min per milligram protein, and the range of values was 0.6 to 16.8 nmol/min per milligram protein. Figure 1*A* shows that the relationship between LPR and GUR was significantly nonzero ($P = .0017$), with a linear correlation coefficient (r^2) of 0.45. There were three outliers beyond 95% confidence intervals, namely, ACC-893, ACC-3171, and ACC-3199, which produced lactate at high rates (13.7, 10.9, and 10.1 nmol/min per milligram), yet consumed glucose at relatively low rates (2.0, 1.1, and 2.2 nmol/min per milligram), respectively. When these were excluded from analysis, the linear correlation coefficient increased to 0.85, suggesting that, for the remaining cells, the lactate was derived from glucose through glycolysis.

These results show that there is a wide range of glycolytic phenotypes among the 12 primary breast tumor lines. Cell line ACC-2715 had the lowest GUR and LPR, whereas ACC-812 and ACC-2150 had highest glycolytic activity (Table 2). Among the other cells, the dynamic ranges were approximately fourfold for both GUR and LPR. A dynamic range of 4.3-fold for glucose trapping is consistent with specific uptake values observed by FdG-PET in clinical studies with breast cancer patients [25].

Table 2. Glycolytic Phenotype of Breast Tumor Lines.

Cell Line	Lactate Production (nmol/min per milligram)	Glucose Uptake (nmol/min per milligram)	GLUT-1 mRNA (×10^5 Copies Relative to Actin mRNA)	GLUT-3 mRNA (×10^5 Copies Relative to Actin mRNA)
ACC-732	4.9 (0.7)	1.9 (0.39)	12.7	0.7
ACC-812	16.8 (1.1)	5.6 (1.0)	21.8	0.0
ACC-893	13.7 (1.7)	2.0 (0.46)	17.6	2.5
ACC-1179	7.6 (1.2)	1.4 (0.30)	27.5	4.1
ACC-2087	9.2 (1.6)	2.2 (0.28)	18.3	2.5
ACC-2150	10.2 (0.8)	4.7 (0.44)	5.4	1.0
ACC-2648	5.8 (1.0)	2.3 (0.55)	12.2	2.3
ACC-2715	0.6 (0.02)	0.6 (0.17)	8.8	2.6
ACC-2925	3.9 (0.6)	1.5 (0.26)	7.4	0.5
ACC-3133	6.0 (0.6)	1.8 (0.33)	3.3	21.4
ACC-3171	10.9 (1.9)	1.1 (0.29)	14.9	1.4
ACC-3199	10.1 (1.4)	2.2 (0.08)	12.8	0.0
MDA-mb-435	11.8 (0.3)	1.7 (0.06)	25.0	110.0
MDA-mb-231	18.9 (1.8)	3.1 (0.33)	4.1	120.9

Mean (SEM) of LPRs, GURs, GLUT-1 mRNA, and GLUT-3 mRNA levels ($n \geq 3$).

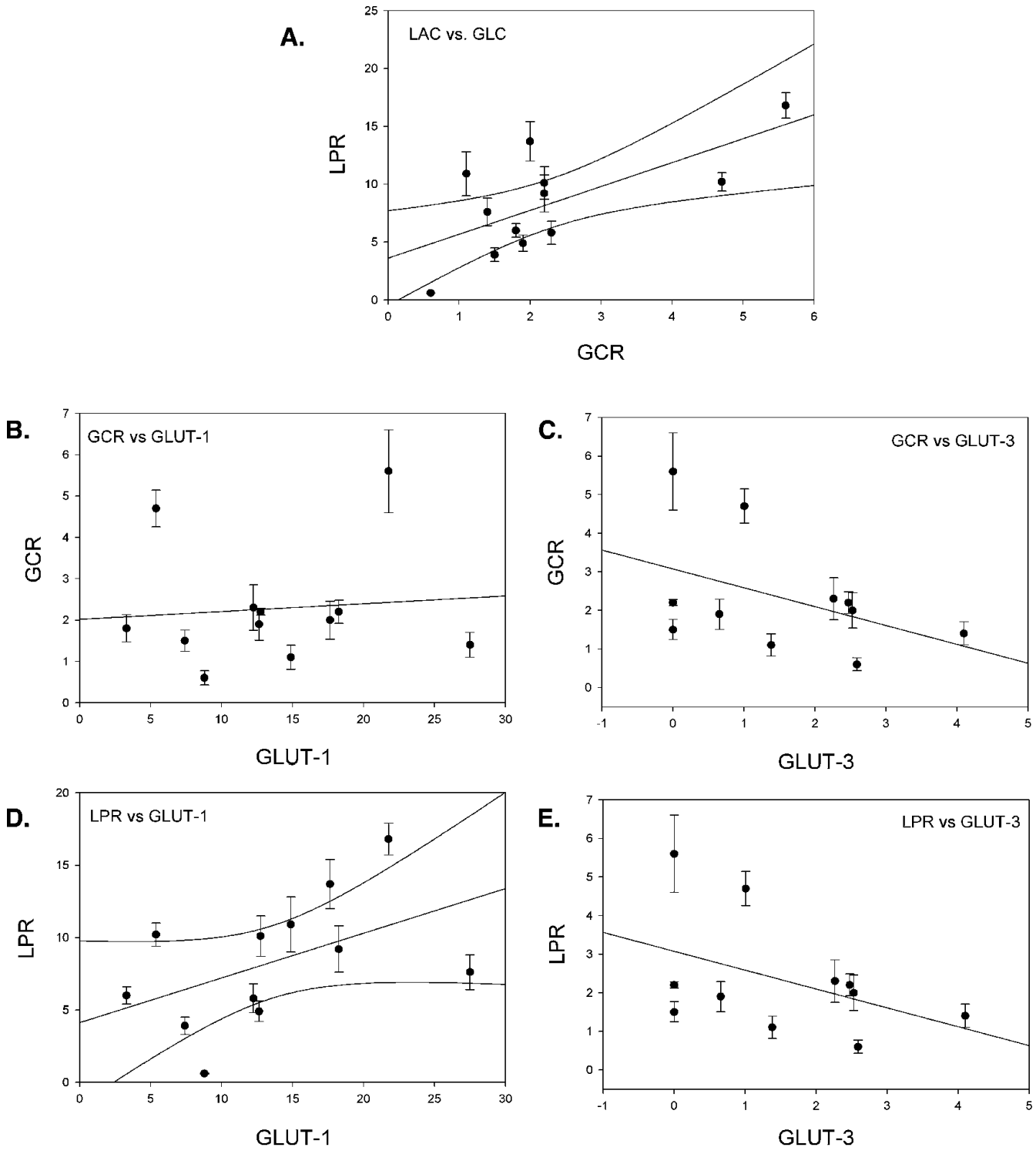

Figure 1. Corelationships between glycolytic markers in breast tumor lines. Linear correlations in the 12 primary breast tumor lines between LPRs and GURs (P = .0173; A), GURs and GLUT-1 mRNA levels (B), GUR and GLUT-3 mRNA levels (C), LPRs and GLUT-1 mRNA levels (D), and lactate production and GLUT-3 mRNA (E).

GLUT-1 mRNA Expression in Low-Passage Breast Tumor Lines

Glucose uptake is regulated by glucose transporters expressed on the cell surface and it represents a rate-limiting step in glycolysis. The rate of uptake is controlled primarily by transporter levels, and this can be reflected by transporter mRNA expression [52,59]. Consequently, glucose transporter mRNA expression levels were determined and quantitatively compared to the kinetic studies. Both GLUT-1 and GLUT-3 expressions were investigated, because these glucose transporters have been associated with uptake of glucose in cancers and exhibit high affinities for both glucose and FdG [60,61]. GLUT-3 levels were low in all primary cell lines, except ACC-3133 that expressed levels exceeding that of MDA-mb-231. GLUT-3 mRNA levels showed a negative, yet insignificant, correlation to both GUR

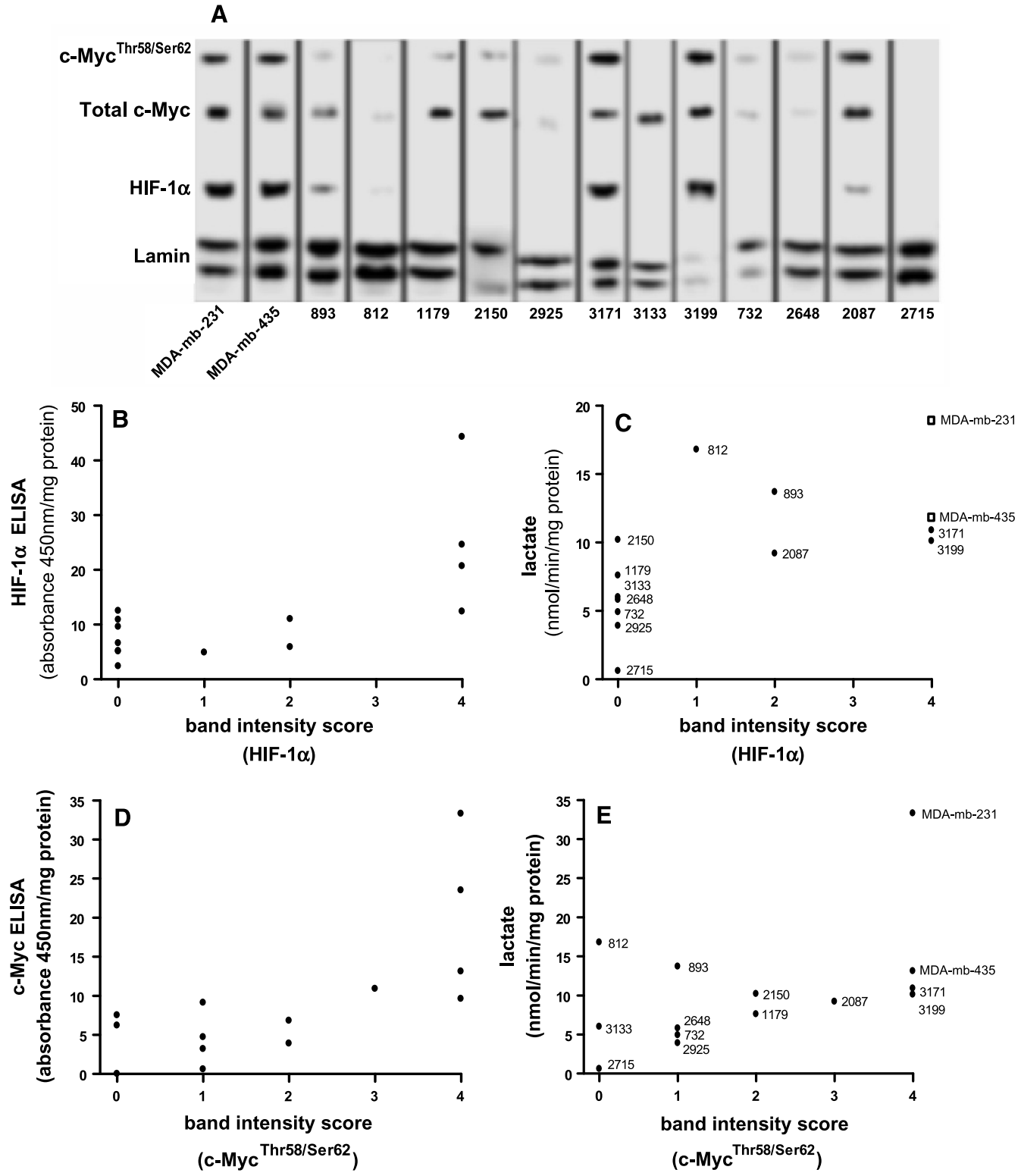

Figure 2. Nuclear expression of phosphorylated c-Myc and HIF-1α. Immunoblot analysis of c-Myc$^{Thr58/Ser62}$, total c-Myc, HIF-1α, and lamin loading from nuclear extracts of ACC-cell lines (A). These data were correlated to activities, as measured by ELISA (B, D) and LPR (C, E).

and LPR (Figure 1, *C* and *E*). GLUT-1 is often overexpressed in malignant cancers and is a negative prognostic marker in breast cancer [25,62–64]. GLUT-1 mRNA levels ranged approximately eightfold, from 3.3 to 27.5 × 10^{-5} copies relative to actin mRNA. GLUT-1 levels were more linear to LPR (Figure 1*D*) than to GUR (Figure 1*B*), but this analysis was not statistically significant.

Evaluation of Nuclear HIF-1α and Phosphorylated c-Myc with Aerobic Glycolysis

Hypoxia-inducible factor 1 alpha is a subcomponent of the heterodimeric HIF-1 transcription factor. It is constitutively produced in the cytoplasm but rapidly degraded by an ubiquitin-mediated system when oxygen is present. If oxygen tension becomes critically low, HIF-1α accumulates,

is phosphorylated, and is translocated to the nucleus where it combines with the HIF-1β/ARNT DNA binding component [43,44,65–67]. Hypoxia-inducible factor 1 coordinately induces the expression of glycolytic enzymes, including the GLUT-1 glucose transporter [68–70].

Nuclear HIF-1α expression under normoxic conditions was examined in each of the breast tumor lines by Western immunoblot analysis (Figure 2*A*). The HIF-1α signal was observed in 5 of 12 primary cell lines. Band intensities were scored from 1 to 4, with 1 being weak staining (ACC-812 cells) and 4 representing high levels (ACC-3171 and ACC-3199 cells). ACC-2087 and ACC-893 cells had intermediate HIF levels (score 2). Both of the stable cell lines (MDA-mb-231 and MDA-mb-435) exhibited strong HIF-1α staining. Nuclear HIF-1α levels were also examined by ELISA. Although we observed a wide range of variability in the ELISA test, we were still able to ascertain a significant association with the Western blot data, confirming the viability of the Western blot analysis results (Figure 2*B*). Cell lines that ranked as a 4 in the Western blot analysis had significantly higher ELISA values compared to cell lines that scored 0, 1, and 2 ($P = .001$).

The HIF-1α status of the primary cell lines was also compared to LPRs, as shown in Figure 2*C*. The two primary cell lines with the highest average LPR (ACC-812 and ACC-893) were only weakly positive for HIF-1α. It may be noteworthy that these were the only two cell lines in this panel that were isolated from primary tumors and not metastases. It is possible that HIF-2α is responsible for glycolytic regulation under normoxia in these cell lines [71]. Our investigations discovered that HIF-2α was expressed in cell line ACC-812 but not in ACC-893 (Figure 3). All of the cell lines positive for HIF-1α staining exhibited higher LPRs compared to cells that did not express measurable levels of HIF-1α ($P = .038$). Somewhat surprisingly, there was no correlation between measurable HIF-1α levels and GURs. The HIF-1α–positive and –negative cells had mean ± SEM GURs of 2.62 ± 0.77 and 2.02 ± 0.49, respectively ($P = .26$; $\alpha = 0.05$, one-sided with equal variance).

The c-Myc transcription factor has been implicated in regulating glycolysis in tumor cells through transactivation of lactate dehydrogenase A [48], up-regulation of GLUT-1 genes [47], and coordinate induction of all glycolytic enzymes [46]. C-Myc is regulated by phosphorylation at Thr58 and Ser62 residues, which facilitates binding to DNA and initiation of transcription [72]. Nuclear extracts from cell lines grown under normoxia were probed with antibodies against phosphorylated c-Myc$^{Thr58/Ser62}$ along with total c-Myc levels (Figure 2*A*). Total c-Myc was detected in all cell lines except for ACC-2715. Phosphorylated c-Myc was observed in all cells except ACC-3133 and ACC-2715, with strongest intensities in ACC-3171, ACC-3199, and ACC-2087 cells. The stable lines MDA-mb-231 and MDA-mb-435 also stained strongly for phosphorylated c-Myc. Cells lines from the Western blots were scored in the same manner as the HIF-1α Western blots and compared to the results from an ELISA measuring c-Myc binding to consensus sequence DNA. As shown in Figure 2*D*, the findings from these analyses were similar to the HIF-1α analysis. The cell lines that ranked as a 4 in the Western blot analysis had significantly higher ELISA absorbance values than cell lines ranked as a 0, 1, 2, and 3 ($P = .0018$).

As with the HIF-1α analysis, phosphorylated c-Myc status was compared to LPRs (Figure 2*E*). Here, we also observed a strong association between glycolytic phenotype and phosphorylated c-Myc status. However, as previously mentioned, cell lines ACC-812 and ACC-893 were clear outliers, with unusually high LPRs. Cell lines with the highest phosphorylated c-Myc signals (ACC-2087, ACC-3171, and ACC-3199) had significantly higher LPR compared to cell lines with weaker or negatively phosphorylated c-Myc signals ($P = .038$). Notably, in cell lines ACC-812 and ACC-893, it is clear that neither HIF nor Myc was involved in regulating aerobic glycolysis in these cell lines. For the other cells, these findings suggest a role for both HIF-1 and c-Myc activation in maintaining the Warburg effect in breast cancer.

Akt Does Not Correlate with Glycolysis

The serine/threonine kinase, Akt is activated by phospholipid binding and activation loop phosphorylation at Thr308 by PDK1 and by phosphorylation within the carboxy-terminus at Ser473 [73]. Akt has been shown to regulate glycolysis at several steps through posttranscriptional mechanisms. Akt localizes GLUT-1 to the cell surface and the maintenance of hexokinase function activity [74]. This activity has been shown to regulate aerobic glycolysis in tumor cells. For example, murine pro–B-cell lymphoid cells transformed with inducible Akt demonstrate up-regulated glucose uptake *in vivo*, and Akt-transformed human glioblastoma cells metabolize glucose in correlation with Akt activity *in vitro* [49]. Whole-cell extracts from breast tumor lines were analyzed for the expression of activated Ser473 pAkt [73] (Figure 4*A*) by the same methods used previously for the c-Myc analysis. Total Akt was observed in all breast tumor lines. Phosphorylated Akt levels were observed in all cell lines except ACC-3199, ACC-2648, and ACC-732. Cell lines ACC-2925, ACC-2150, and ACC-893 expressed the highest intensities of Akt^{Ser473}. The ratio of mean band intensities between pAkt and total Akt was determined using the measure function in the ImageJ downloadable application [75].

Expression of pAkt as a ratio to total Akt was compared to LPRs in each cell line (Figure 4*B*). A linear regression analysis determined that there was no significant deviation from zero in this comparison ($P = .87$). We conclude that transactivation of Akt is not necessary to regulate aerobic glycolysis in breast cancer cells and its activity—in particular reference to cell line ACC-2925—does not seem to enhance cellular glycolysis under normoxic conditions.

Pharmacologic Manipulation of c-Myc and HIF-1α

ACC-3199 cells were cultured overnight in serum-free medium to reduce activated c-Myc levels. Cultures were then treated with TPA, a reagent that acutely activates c-Myc through kinase C–mediated phosphorylation [76]. 2-*O*-Tetradecanoylphorbol-13-acetate caused a nearly twofold increase in lactate production after a 2-hour incubation ($P = .004$) along with a corresponding increase in c-Myc$^{Thr58/Ser62}$

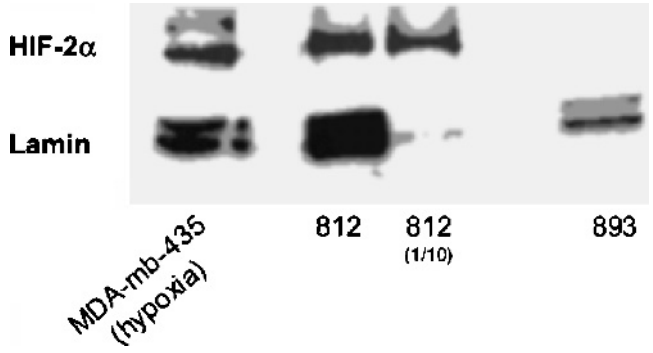

Figure 3. Nuclear expression of HIF-2α. Immunoblot analysis of HIF-2α and lamin loading from nuclear extracts of ACC-812 and ACC-893.

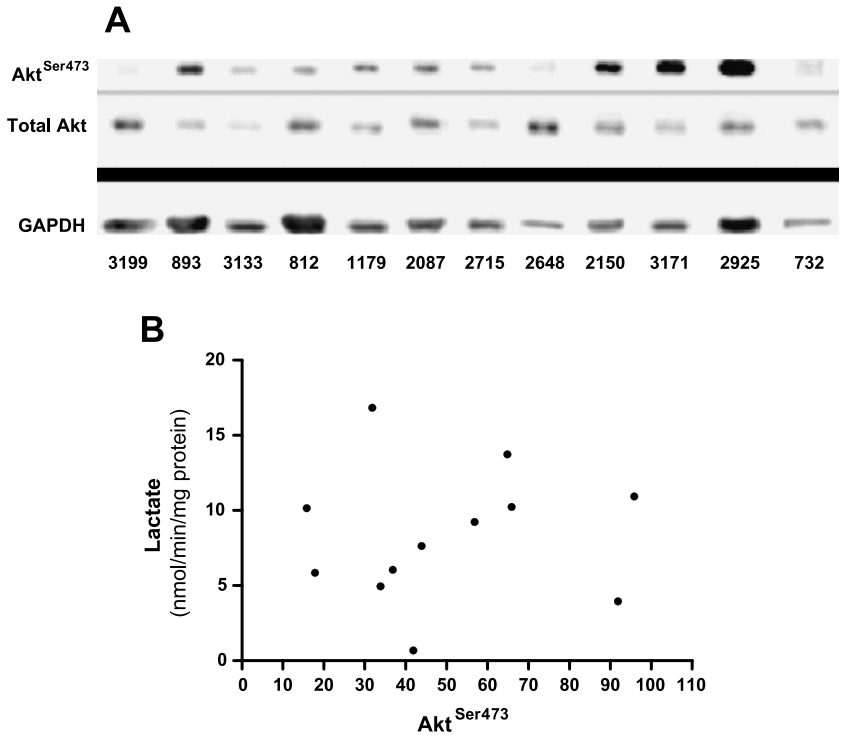

Figure 4. Nuclear expression of pAkt and total Akt. (A) Immunoblot of Ser473 pAkt, total Akt, and GAPDH control from nuclear extracts of ACC breast tumor lines. (B) Correlation of pAkt mean band intensities normalized to total Akt expression and lactate production, $P = .87$.

levels (Figure 5). The blots were stripped with 0.2 M NaOH and gentle shaking for 10 minutes and were reprobed for HIF-1α. The process was repeated for nuclear lamin A/C loading control. Notably, HIF-1α expression was present under both conditions, and levels were relatively unchanged by TPA treatment (Figure 5).

These results suggest two possible mechanisms of glycolytic up-regulation induced by TPA treatment. Activity of phospho–c-Myc induced by TPA may have directly increased glycolytic activity in ACC-3199 cells. Alternatively, a regulatory dynamic relationship between c-Myc and HIF-1 may exist.

To further test this relationship, inhibition of HIF-1α was accomplished with PX-478, a reagent that targets HIF-1α, possibly through mRNA stability [56]. MDA-mb-231 cells were cultured under hypoxic conditions (O_2 = 2%) for 24 hours to maximally up-regulate HIF-1α expression and treated with 20 and 40 mg/ml of PX-478. Both GUR and HIF-1α coordinately and significantly decreased in a dose-dependent manner (Figure 6).

Tumor Formation

As a final test to characterize the phenotypes exhibited by this panel of cell lines, each cell line was inoculated bilaterally into mammary fat pads of two female SCID mice (four inocula per cell line) to test their ability to grow as tumors. Of 12 cell lines, only 4 formed tumors: ACC-3199, ACC-3171, ACC-2150, and ACC-893. This observation is consistent with other reports discussing investigations working with primary breast cancer cell lines in animals [77]. To establish a stable cell line without genetic drift as seen typically in low-passage cell lines, the tumors that grew were reimplanted twice into more SCID mice for a total of three passages. ACC-2150 and ACC-893 failed to grow after reimplantation. Hence, only ACC-3199 and ACC-3171 were able to grow reproducibly as tumors in SCID mice. Notably, their pAkt status did not change during growth: i.e. ACC-3199 remained pAkt-negative, whereas ACC-3171 was strongly pAkt-positive (Figure 7). Both of these cell lines were positive for phospho–c-Myc and HIF-1α, and these molecular phenotypes also did not change during *in vivo* selection (data not shown).

Discussion

Whereas FdG uptake is uniformly high in aggressive and metastatic cancers, its use as a pathodiagnostic agent in breast cancer is limited to its high variability. The purpose of these studies was to

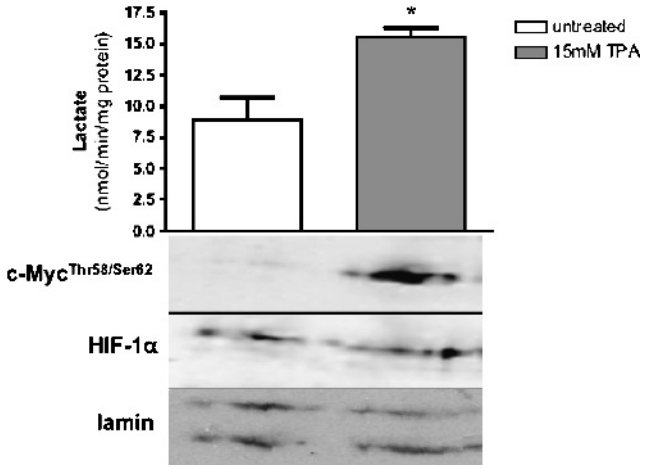

Figure 5. Expression of phosphorylated c-Myc, HIF-1α, and lactate production in TPA-treated breast tumor cell line. Increase of c-Myc expression and lactate production when ACC-3199 cells are treated with 15 mM TPA for 2 hours.

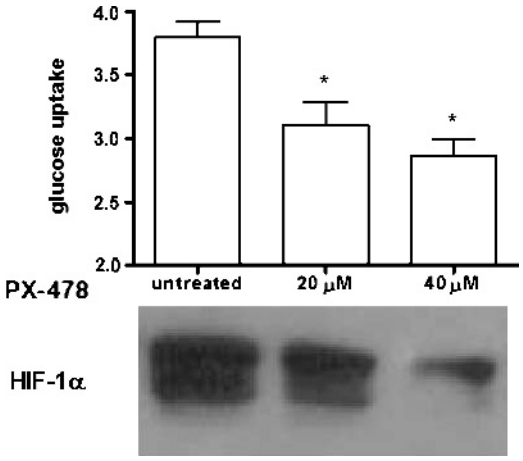

Figure 6. Effect of PX-478 on HIF-1α and glycolysis. Dose-dependent decrease in glucose uptake in MDA-mb-231 cells (20 and 40 μg/ml) after 24 hours of treatment with PX-478 under hypoxia (O_2 = 2%). *P = .01 compared to untreated controls.

investigate the molecular mechanisms underlying FdG uptake variability. In this study, we examined glycolytic phenotypes and the possible relationships between aerobic glycolysis and expression of oncogenic factors associated with malignancy. This investigation focused on 12 low-passage breast tumor lines and included two established metastatic breast tumor lines for comparison. Both glucose uptake and lactic acid production were variable, but highly correlated, among the individual cell lines. This is consistent with the observed variability of FdG uptake by PET scanning in breast cancer patients [2,7,18, 20–27]. Breast carcinomas with higher rates of FdG uptake have the poorest prognosis [2–5].

Elevated FdG uptake may be associated with the Warburg effect. The relationship between the Warburg effect and malignancy suggests a possible selective advantage to cancer cells, but a proliferative advantage is not apparent. Glycolysis is energetically less efficient than oxidative phosphorylation and produces toxic byproducts. Selection of the Warburg effect for purposes of energetic fitness is not logical considering that aerobic glycolysis is an existing metabolic function in all eukaryotic cells. It must be considered, therefore, that aerobic glycolysis is not selected for production of ATP. A relatively minor fraction (<30%) of a cancer cell's aerobic ATP production is derived from glycolysis according to mass balance analyses [78]. There are explanations, other than bioenergetics, which address this observation. Glycolysis produces hydrogen ions, and increased acidity offers a selective advantage to invading tumor cells. Alternatively, Glucose metabolism may occur through the pentose phosphate pathway, providing anabolic substrates such as ribose for nucleic acid synthesis as well as reducing equivalents (NADPH) to combat reactive oxygen species [79,80]. This material is discussed in greater detail in a recent review by Gillies and Gatenby [81].

In most of the cell lines, GUR correlated to LPR, indicating that either measurement would reflect rates of glucose metabolism for almost all cells. Outliers in this analysis were ACC-893, ACC-3171, and ACC-3199, which all produced lactate at rates higher than would be expected from their GURs. Interestingly, these three cell lines were also tumorigenic in SCID mice. High rates of lactate production by these cells may be due to additional lactate-producing pathways such as enhanced glutaminolysis [82], and this remains to be confirmed. The cell line ACC-812 exhibited the highest rate of glycolysis by either measurement yet had lower than expected levels of both HIF-1α and c-Myc (Figure 2). These cells were isolated from primary tumor sites compared to the others that were isolated from lymph nodes or pleural effusions. ACC-812 cells were also not tumorigenic in SCID mice.

Glucose transporter levels are a common end point in cancer studies due to high expression in tumor malignancy and its positive correlation with FdG-PET studies [25,64]. In previous studies with established breast tumor lines, others and we have noted that GLUT-1 mRNA expression can reflect GLUT-1 protein expression [52,59], yet these results can not be extrapolated to the current study. This could be due to a combination of several factors. Although there is evidence supporting a correlation between mRNA and protein expression [83], there may be unknown posttranscriptional modifications or protein half-lives that would not be reflective of the true level of active glucose transporters when making comparisons to transcript levels. This phenomenon has been observed in cultured cells with disrupted oxidative phosphorylation [84]. This was noted in our own experiments as well. For example, cell lines ACC-1179, ACC-893, and ACC-3199 expressed comparably higher levels of GLUT-1 message but exhibited weak GLUT-1 protein expression (Figure W1). GLUT-3 could also contribute to GUR, and it is highly expressed in the stable cell lines MDA-mb-231 and MDA-mb-435. However, in the current panel, there is no significant relationship between expression of this gene and either GUR or LPR (Figure 1).

Both aerobic glycolysis and GLUT-1 levels may be stimulated by a host of oncogenic factors, such as HIF-1α [50–54], c-Myc [47,48],

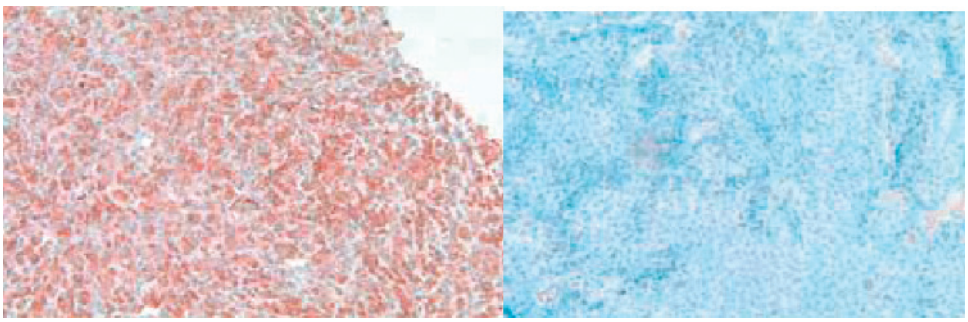

Figure 7. Immunohistochemistry for pAkt in ACC-3171 and ACC-3199 tumors. Breast tumor cell lines grown in SCID mice and then reimplanted into new SCID mice were stained for pAkt. ACC-3171 demonstrated a positive staining for pAkt, whereas ACC-3199 was negative for pAkt.

or Akt [49]. We noted that earlier reports have shown HIF-1α levels, measured with histologic diagnosis, did not correlate well with increased FdG uptake measured by PET in breast cancers [25]. Hence, we were concerned that the relationship between HIF-1α and the Warburg effect was particular to cell lines that were established in culture. To examine this, we developed a series of low-passage breast cancer lines, with the rationale that they would more adequately represent cells from *in vivo* tumors. We observed that cell lines exhibiting the highest relative rates of aerobic glycolysis were positive for nuclear HIF-1α. Notably, cell lines with lowest glycolytic rates were negative for the expression of nuclear HIF-1α. Clear exceptions to these observations are cell lines ACC-812 and ACC-893, both of which were highly glycolytic but expressed low or negative levels of normoxic HIF-1α. Although it does not seem that HIF-1α is involved in glycolytic regulation of these two cell lines, it is possible that HIF-1 homologues such as HIF-2α may be up-regulated in these cells [71] and contribute to glycolytic regulation under normoxia. We tested for the expression of this factor in ACC-812 and ACC-893 and discovered that the expression of HIF-2α was indeed positive and comparable to a nuclear extract from metastatic breast tumor line (MDA-mb-435) that had been cultured under hypoxic conditions (O_2 at 2% for 24 hours). We did not observe any expression of HIF-2α in ACC-893 (Figure 3). Another possibility for the Warburg effect in these cell lines—and this remains to be tested—is the regulation by a cell cycle regulator ubiquitin ligase with the F-box protein Grr1 (SCF^{Grr1}), which has been shown to target transcription factors involved in regulating glycolysis [85].

It was previously reported that transactivation of c-Myc is dependent on its phosphorylation at Thr58 and Ser62 [72]. This event is somewhat complicated in that phosphorylation of c-Myc at Ser62 promotes stabilization and accumulation of c-Myc and conversely, phosphorylation of c-Myc at Thr58 accelerates c-Myc ubiquitination and proteolytic degradation [86]. Dephosphorylation of Ser62 is required, however, for degradation to occur [87]. We examined the expression of $c\text{-}Myc^{Thr58/Ser62}$ and observed a general correspondence with aerobic glycolysis in the primary breast tumor lines. These data corresponded with the ELISA experiments that measured c-Myc binding to an immobilized oligonucleotide containing the c-Myc consensus binding site (5′-CACGTG-3′; Figure 2*D*), thus we interpret $c\text{-}Myc^{Thr58/Ser62}$ expression to indicate c-Myc activity. There was a higher expression of $c\text{-}Myc^{Thr58/Ser62}$ in glycolytic lines ACC-3199, ACC-3171, and ACC-2087, which were comparable to the stable cell lines MDA-mb-231 and MDA-mb-435. We also noted lower or negative c-Myc activity in cells with lowest glycolytic rates. Similar to HIF-1α, cell lines 812 and 893 expressed low levels of phosphorylated c-Myc but had the highest LPRs, suggesting that other factors are responsible for regulating glucose metabolism in these cell lines.

We also examined pAkt expression in this panel. Phosphorylated Akt expression was examined along with total Akt levels relative to glyceraldehyde-3-phosphate dehydrogenase (GAPDH), a common cytoplasmic protein loading control. GAPDH expression was robust in all cell lines but variable. This may be due to the role of GAPDH in glycolysis. Therefore, the levels of pAkt expression in cells were also expressed as a ratio between pAkt and total Akt from the band intensities in the Western blot (Figure 4*A*). Both pAkt/total Akt and pAkt/GAPDH ratios were compared to lactate production and showed no significant relationship.

At the outset of these studies, cross talk between c-Myc and HIF-1 had not previously been seen. We began to examine this in more detail when it was reported in two systems by Semenza and Dang [55,88]. To test the hypothesis that c-Myc and HIF-1α can regulate the glycolytic phenotype in breast cancer cells, c-Myc was activated with TPA. 2-*O*-Tetradecanoylphorbol-13-acetate induced both phosphorylated c-Myc along with a significant increase in lactate production. Effects of TPA on c-Myc phosphorylation are consistent with previous reports [76]. It should be noted that HIF-1α levels are also reportedly affected by TPA [89,90]. One study [89] provided evidence that phorbol-12-myristate-13-acetate induced HIF-1 through mitogen-activated protein/extracellular signal–regulated kinase 1 (MEK-1) signaling. Transcription factor c-Myc can activate the MEK-1 pathway, at least in rhabdomyosarcoma cells [91]. To test if inhibition of these transcription factors would down-regulate glycolysis, HIF-1α was inhibited with PX-478 [56], and this led to dose-dependent decreases in both HIF-1α and glucose uptake. Hence, we conclude that the Warburg effect in these cell lines is also associated with elevated HIF-1α levels and that the effect is amplified by c-Myc. Because this does not explain the lack of correlation observed *in vivo*, we also conclude that *in vivo* FdG uptake can be driven by other pathways in addition to HIF-1α.

We have recently developed a model to explain why cancers have high glycolysis [32]. This model predicts that expression of a glycolytic phenotype is essential to cancer progression and predicts that this can be achieved through multiple mechanisms that can be different even within specific types of cancers. The results of this study are consistent with this prediction in that two transcription factors, c-Myc and HIF-1, seem to be mutually associated with regulation of aerobic glycolysis.

Acknowledgments

The authors thank Garth Powis for kindly providing us with the PX reagents used in this study. The authors also thank Dave Morse for intellectual contribution, Alfred Gallegos and Amanda Baker for technical assistance, and Merry Warner for administrative contributions.

References

[1] Jemal A, Murray T, Ward E, Samuels A, Tiwari RC, Ghafoor A, Feuer EJ, and Thun MJ (2005). Cancer statistics, 2005. *CA Cancer J Clin* **55** (1), 10–30.

[2] Kumar R and Alavi A (2004). Fluorodeoxyglucose-PET in the management of breast cancer. *Radiol Clin North Am* **42** (6), 1113–1122, ix.

[3] Kumar R, Zhuang H, Schnall M, Conant E, Damia S, Weinstein S, Chandra P, Czerniecki B, and Alavi A (2006). FDG PET positive lymph nodes are highly predictive of metastasis in breast cancer. *Nucl Med Commun* **27** (3), 231–236.

[4] Moon DH, Maddahi J, Silverman DH, Glaspy JA, Phelps ME, and Hoh CK (1998). Accuracy of whole-body fluorine-18-FDG PET for the detection of recurrent or metastatic breast carcinoma. *J Nucl Med* **39** (3), 431–435.

[5] Oshida M, Uno K, Suzuki M, Nagashima T, Hashimoto H, Yagata H, Shishikura T, Imazeki K, and Nakajima N (1998). Predicting the prognoses of breast carcinoma patients with positron emission tomography using 2-deoxy-2-fluoro[^{18}F]-D-glucose. *Cancer* **82** (11), 2227–2234.

[6] Ueda S, Tsuda H, Asakawa H, Shigekawa T, Fukatsu K, Kondo N, Yamamoto M, Hama Y, Tamura K, Ishida J, et al. (2008). Clinicopathological and prognostic relevance of uptake level using ^{18}F-fluorodeoxyglucose positron emission tomography/computed tomography fusion imaging (^{18}F-FDG PET/CT) in primary breast cancer. *Jpn J Clin Oncol* **38** (4), 250–258.

[7] Adler LP, Crowe JP, al-Kaisi NK, and Sunshine JL (1993). Evaluation of breast masses and axillary lymph nodes with [F-18] 2-deoxy-2-fluoro-D-glucose PET. *Radiology* **187** (3), 743–750.

[8] Avril N, Dose J, Janicke F, Bense S, Ziegler S, Laubenbacher C, Romer W, Pache H, Herz M, Allgayer B, et al. (1996). Metabolic characterization of breast tumors with positron emission tomography using F-18 fluorodeoxyglucose. *J Clin Oncol* **14** (6), 1848–1857.

[9] Czernin J and Phelps ME (2002). Positron emission tomography scanning: current and future applications. *Annu Rev Med* **53**, 89–112.

[10] Gambhir SS, Czernin J, Schwimmer J, Silverman DH, Coleman RE, and Phelps ME (2001). A tabulated summary of the FDG PET literature. *J Nucl Med* **42** (5 Suppl), 1S–93S.

[11] Adler LP, Faulhaber PF, Schnur KC, Al-Kasi NL, and Shenk RR (1997). Axillary lymph node metastases: screening with [F-18]2-deoxy-2-fluoro-D-glucose (FDG) PET. *Radiology* **203** (2), 323–327.

[12] Avril N, Dose J, Janicke F, Ziegler S, Romer W, Weber W, Herz M, Nathrath W, Graeff H, and Schwaiger M (1996). Assessment of axillary lymph node involvement in breast cancer patients with positron emission tomography using radiolabeled 2-(fluorine-18)-fluoro-2-deoxy-D-glucose. *J Natl Cancer Inst* **88** (17), 1204–1209.

[13] Greco M, Crippa F, Agresti R, Seregni E, Gerali A, Giovanazzi R, Micheli A, Asero S, Ferraris C, Gennaro M, et al. (2001). Axillary lymph node staging in breast cancer by 2-fluoro-2-deoxy-D-glucose-positron emission tomography: clinical evaluation and alternative management. *J Natl Cancer Inst* **93** (8), 630–635.

[14] Rostom AY, Powe J, Kandil A, Ezzat A, Bakheet S, el-Khwsky F, el-Hussainy G, Sorbris R, and Sjoklint O (1999). Positron emission tomography in breast cancer: a clinicopathological correlation of results. *Br J Radiol* **72** (863), 1064–1068.

[15] Schirrmeister H, Kuhn T, Guhlmann A, Santjohanser C, Horster T, Nussle K, Koretz K, Glatting G, Rieber A, Kreienberg R, et al. (2001). Fluorine-18 2-deoxy-2-fluoro-D-glucose PET in the preoperative staging of breast cancer: comparison with the standard staging procedures. *Eur J Nucl Med* **28** (3), 351–358.

[16] Smith IC, Ogston KN, Whitford P, Smith FW, Sharp P, Norton M, Miller ID, Ah-See AK, Heys SD, Jibril JA, et al. (1998). Staging of the axilla in breast cancer: accurate *in vivo* assessment using positron emission tomography with 2-(fluorine-18)-fluoro-2-deoxy-D-glucose. *Ann Surg* **228** (2), 220–227.

[17] Utech CI, Young CS, and Winter PF (1996). Prospective evaluation of fluorine-18 fluorodeoxyclucose positron emission tomography in breast cancer for staging of the axilla related to surgery and immunocytochemistry. *Eur J Nucl Med* **23** (12), 1588–1593.

[18] van der Hoeven JJ, Hoekstra OS, Comans EF, Pijpers R, Boom RP, van Geldere D, Meijer S, Lammertsma AA, and Teule GJ (2002). Determinants of diagnostic performance of [F-18]fluorodeoxyglucose positron emission tomography for axillary staging in breast cancer. *Ann Surg* **236** (5), 619–624.

[19] Yutani K, Shiba E, Kusuoka H, Tatsumi M, Uehara T, Taguchi T, Takai SI, and Nishimura T (2000). Comparison of FDG-PET with MIBI-SPECT in the detection of breast cancer and axillary lymph node metastasis. *J Comput Assist Tomogr* **24** (2), 274–280.

[20] Avril N, Rose CA, Schelling M, Dose J, Kuhn W, Bense S, Weber W, Ziegler S, Graeff H, and Schwaiger M (2000). Breast imaging with positron emission tomography and fluorine-18 fluorodeoxyglucose: use and limitations. *J Clin Oncol* **18** (20), 3495–3502.

[21] Eubank WB and Mankoff DA (2005). Evolving role of positron emission tomography in breast cancer imaging. *Semin Nucl Med* **35** (2), 84–99.

[22] Wahl RL, Cody RL, Hutchins GD, and Mudgett EE (1991). Primary and metastatic breast carcinoma: initial clinical evaluation with PET with the radiolabeled glucose analogue 2-[F-18]-fluoro-2-deoxy-D-glucose. *Radiology* **179** (3), 765–770.

[23] Avril N, Bense S, Ziegler SI, Dose J, Weber W, Laubenbacher C, Romer W, Janicke F, and Schwaiger M (1997). Breast imaging with fluorine-18-FDG PET: quantitative image analysis. *J Nucl Med* **38** (8), 1186–1191.

[24] Avril N, Menzel M, Dose J, Schelling M, Weber W, Janicke F, Nathrath W, and Schwaiger M (2001). Glucose metabolism of breast cancer assessed by ^{18}F-FDG PET: histologic and immunohistochemical tissue analysis. *J Nucl Med* **42** (1), 9–16.

[25] Bos R, van Der Hoeven JJ, van Der Wall E, van Der Groep P, van Diest PJ, Comans EF, Joshi U, Semenza GL, Hoekstra OS, Lammertsma AA, et al. (2002). Biologic correlates of (18)fluorodeoxyglucose uptake in human breast cancer measured by positron emission tomography. *J Clin Oncol* **20** (2), 379–387.

[26] Buck A, Schirrmeister H, Kuhn T, Shen C, Kalker T, Kotzerke J, Dankerl A, Glatting G, Reske S, and Mattfeldt T (2002). FDG uptake in breast cancer: correlation with biological and clinical prognostic parameters. *Eur J Nucl Med Mol Imaging* **29** (10), 1317–1323.

[27] Kumar R, Chauhan A, Zhuang H, Chandra P, Schnall M, and Alavi A (2006). Clinicopathologic factors associated with false negative FDG-PET in primary breast cancer. *Breast Cancer Res Treat* **98** (3), 267–274.

[28] Warburg O (1930). *The Metabolism of Tumours.* London, England: Constable.

[29] Shaw RJ (2006). Glucose metabolism and cancer. *Curr Opin Cell Biol* **18** (6), 598–608.

[30] Cherk MH, Foo SS, Poon AM, Knight SR, Murone C, Papenfuss AT, Sachinidis JI, Saunder TH, O'Keefe GJ, and Scott AM (2006). Lack of correlation of hypoxic cell fraction and angiogenesis with glucose metabolic rate in non–small cell lung cancer assessed by ^{18}F-fluoromisonidazole and ^{18}F-FDG PET. *J Nucl Med* **47** (12), 1921–1926.

[31] Rajendran JG, Mankoff DA, O'Sullivan F, Peterson LM, Schwartz DL, Conrad EU, Spence AM, Muzi M, Farwell DG, and Krohn KA (2004). Hypoxia and glucose metabolism in malignant tumors: evaluation by [^{18}F]fluoromisonidazole and [^{18}F]fluorodeoxyglucose positron emission tomography imaging. *Clin Cancer Res* **10** (7), 2245–2252.

[32] Gatenby RA and Gillies RJ (2004). Why do cancers have high aerobic glycolysis? *Nat Rev Cancer* **4** (11), 891–899.

[33] Semenza GL, Artemov D, Bedi A, Bhujwalla Z, Chiles K, Feldser D, Laughner E, Ravi R, Simons J, Taghavi P, et al. (2001). "The metabolism of tumours": 70 years later. *Novartis Found Symp* **240**, 251–260; discussion 260–264.

[34] Gambhir SS (2002). Molecular imaging of cancer with positron emission tomography. *Nat Rev Cancer* **2** (9), 683–693.

[35] Weber WA (2006). Positron emission tomography as an imaging biomarker. *J Clin Oncol* **24** (20), 3282–3292.

[36] Baudelet C, Ansiaux R, Jordan BF, Havaux X, Macq B, and Gallez B (2004). Physiological noise in murine solid tumours using T2*-weighted gradient-echo imaging: a marker of tumour acute hypoxia? *Phys Med Biol* **49** (15), 3389–3411.

[37] Gilead A and Neeman M (1999). Dynamic remodeling of the vascular bed precedes tumor growth: MLS ovarian carcinoma spheroids implanted in nude mice. *Neoplasia* **1** (3), 226–230.

[38] Kimura H, Braun RD, Ong ET, Hsu R, Secomb TW, Papahadjopoulos D, Hong K, and Dewhirst MW (1996). Fluctuations in red cell flux in tumor microvessels can lead to transient hypoxia and reoxygenation in tumor parenchyma. *Cancer Res* **56** (23), 5522–5528.

[39] Raghunand N, Gatenby RA, and Gillies RJ (2003). Microenvironmental and cellular consequences of altered blood flow in tumours. *Br J Radiol* **76 Spec No 1**, S11–S22.

[40] Gatenby RA and Vincent TL (2003). An evolutionary model of carcinogenesis. *Cancer Res* **63** (19), 6212–6220.

[41] Gatenby RA and Gillies RJ (2008). A microenvironmental model of carcinogenesis. *Nat Rev Cancer* **8** (1), 56–61.

[42] Pouyssegur J, Dayan F, and Mazure NM (2006). Hypoxia signalling in cancer and approaches to enforce tumour regression. *Nature* **441** (7092), 437–443.

[43] Semenza GL (1998). Hypoxia-inducible factor 1: master regulator of O_2 homeostasis. *Curr Opin Genet Dev* **8** (5), 588–594.

[44] Semenza GL (2001). HIF-1, O(2), and the 3 PHDs: how animal cells signal hypoxia to the nucleus. *Cell* **107** (1), 1–3.

[45] Gillies R, Robey IF, and Gatenby RA (in press). Causes and consequences of increased glucose consumption in cancers. *J Nucl Med*.

[46] Kim JW, Zeller KI, Wang Y, Jegga AG, Aronow BJ, O'Donnell KA, and Dang CV (2004). Evaluation of *myc* E-box phylogenetic footprints in glycolytic genes by chromatin immunoprecipitation assays. *Mol Cell Biol* **24** (13), 5923–5936.

[47] Osthus RC, Shim H, Kim S, Li Q, Reddy R, Mukherjee M, Xu Y, Wonsey D, Lee LA, and Dang CV (2000). Deregulation of glucose transporter 1 and glycolytic gene expression by c-Myc. *J Biol Chem* **275** (29), 21797–21800.

[48] Shim H, Dolde C, Lewis BC, Wu CS, Dang G, Jungmann RA, Dalla-Favera R, and Dang CV (1997). c-Myc transactivation of LDH-A: implications for tumor metabolism and growth. *Proc Natl Acad Sci USA* **94** (13), 6658–6663.

[49] Elstrom RL, Bauer DE, Buzzai M, Karnauskas R, Harris MH, Plas DR, Zhuang H, Cinalli RM, Alavi A, Rudin CM, et al. (2004). Akt stimulates aerobic glycolysis in cancer cells. *Cancer Res* **64** (11), 3892–3899.

[50] Lu H, Forbes RA, and Verma A (2002). Hypoxia-inducible factor 1 activation by aerobic glycolysis implicates the Warburg effect in carcinogenesis. *J Biol Chem* **277** (26), 23111–23115.

[51] Obach M, Navarro-Sabate A, Caro J, Kong X, Duran J, Gomez M, Perales JC, Ventura F, Rosa JL, and Bartrons R (2004). 6-Phosphofructo-2-kinase (*pfkfb3*) gene promoter contains hypoxia-inducible factor-1 binding sites necessary for transactivation in response to hypoxia. *J Biol Chem* **279** (51), 53562–53570.

[52] Robey IF, Lien AD, Welsh SJ, Baggett BK, and Gillies RJ (2005). Hypoxia-inducible factor-1α and the glycolytic phenotype in tumors. *Neoplasia* **7** (4), 324–330.

[53] Wang V, Davis DA, Haque M, Huang LE, and Yarchoan R (2005). Differential gene up-regulation by hypoxia-inducible factor-1α and hypoxia-inducible factor-2α in HEK293T cells. *Cancer Res* **65** (8), 3299–3306.

[54] Yasuda S, Arii S, Mori A, Isobe N, Yang W, Oe H, Fujimoto A, Yonenaga Y, Sakashita H, and Imamura M (2004). Hexokinase II and VEGF expression in liver tumors: correlation with hypoxia-inducible factor 1α and its significance. *J Hepatol* **40** (1), 117–123.

[55] Zhang H, Gao P, Fukuda R, Kumar G, Krishnamachary B, Zeller KI, Dang CV, and Semenza GL (2007). HIF-1 inhibits mitochondrial biogenesis and cellular respiration in VHL-deficient renal cell carcinoma by repression of C-MYC activity. *Cancer Cell* **11** (5), 407–420.

[56] Welsh S, Williams R, Kirkpatrick L, Paine-Murrieta G, and Powis G (2004). Antitumor activity and pharmacodynamic properties of PX-478, an inhibitor of hypoxia-inducible factor-1α. *Mol Cancer Ther* **3** (3), 233–244.

[57] Hiratsuka M, Senoo T, Kimoto T, and Namba M (1982). An improved short-term culture method for human mammary epithelial cells. *Gann* **73** (1), 124–128.

[58] Pfaffl MW (2001). A new mathematical model for relative quantification in real-time RT-PCR. *Nucleic Acids Res* **29** (9), e45.

[59] Grover-McKay M, Walsh SA, Seftor EA, Thomas PA, and Hendrix MJ (1998). Role for glucose transporter 1 protein in human breast cancer. *Pathol Oncol Res* **4** (2), 115–120.

[60] Burant CF and Bell GI (1992). Mammalian facilitative glucose transporters: evidence for similar substrate recognition sites in functionally monomeric proteins. *Biochemistry* **31** (42), 10414–10420.

[61] Keller K, Strube M, and Mueckler M (1989). Functional expression of the human HepG2 and rat adipocyte glucose transporters in *Xenopus oocytes*. Comparison of kinetic parameters. *J Biol Chem* **264** (32), 18884–18889.

[62] Brown RS and Wahl RL (1993). Overexpression of Glut-1 glucose transporter in human breast cancer. An immunohistochemical study. *Cancer* **72** (10), 2979–2985.

[63] Burnol AF, Leturque A, Loizeau M, Postic C, and Girard J (1990). Glucose transporter expression in rat mammary gland. *Biochem J* **270** (1), 277–279.

[64] Macheda ML, Rogers S, and Best JD (2005). Molecular and cellular regulation of glucose transporter (GLUT) proteins in cancer. *J Cell Physiol* **202** (3), 654–662.

[65] Ivan M, Kondo K, Yang H, Kim W, Valiando J, Ohh M, Salic A, Asara JM, Lane WS, and Kaelin WG Jr (2001). HIFα targeted for VHL-mediated destruction by proline hydroxylation: implications for O_2 sensing. *Science* **292** (5516), 464–468.

[66] Jaakkola P, Mole DR, Tian YM, Wilson MI, Gielbert J, Gaskell SJ, Kriegsheim A, Hebestreit HF, Mukherji M, Schofield CJ, et al. (2001). Targeting of HIF-α to the von Hippel–Lindau ubiquitylation complex by O_2-regulated prolyl hydroxylation. *Science* **292** (5516), 468–472.

[67] Maxwell PH, Wiesener MS, Chang GW, Clifford SC, Vaux EC, Cockman ME, Wykoff CC, Pugh CW, Maher ER, and Ratcliffe PJ (1999). The tumour suppressor protein VHL targets hypoxia-inducible factors for oxygen-dependent proteolysis. *Nature* **399** (6733), 271–275.

[68] Ebert BL, Firth JD, and Ratcliffe PJ (1995). Hypoxia and mitochondrial inhibitors regulate expression of glucose transporter-1 via distinct Cis-acting sequences. *J Biol Chem* **270** (49), 29083–29089.

[69] Maxwell PH, Dachs GU, Gleadle JM, Nicholls LG, Harris AL, Stratford IJ, Hankinson O, Pugh CW, and Ratcliffe PJ (1997). Hypoxia-inducible factor-1 modulates gene expression in solid tumors and influences both angiogenesis and tumor growth. *Proc Natl Acad Sci USA* **94** (15), 8104–8109.

[70] Zelzer E, Levy Y, Kahana C, Shilo BZ, Rubinstein M, and Cohen B (1998). Insulin induces transcription of target genes through the hypoxia-inducible factor HIF-1α/ARNT. *EMBO J* **17** (17), 5085–5094.

[71] Zhong H, De Marzo AM, Laughner E, Lim M, Hilton DA, Zagzag D, Buechler P, Isaacs WB, Semenza GL, and Simons JW (1999). Overexpression of hypoxia-inducible factor 1α in common human cancers and their metastases. *Cancer Res* **59** (22), 5830–5835.

[72] Gupta S, Seth A, and Davis RJ (1993). Transactivation of gene expression by Myc is inhibited by mutation at the phosphorylation sites Thr-58 and Ser-62. *Proc Natl Acad Sci USA* **90** (8), 3216–3220.

[73] Alessi DR, Andjelkovic M, Caudwell B, Cron P, Morrice N, Cohen P, and Hemmings BA (1996). Mechanism of activation of protein kinase B by insulin and IGF-1. *EMBO J* **15** (23), 6541–6551.

[74] Rathmell JC, Fox CJ, Plas DR, Hammerman PS, Cinalli RM, and Thompson CB (2003). Akt-directed glucose metabolism can prevent Bax conformation change and promote growth factor-independent survival. *Mol Cell Biol* **23** (20), 7315–7328.

[75] Rasband WS (1997–2007). *ImageJ*. Bethesda, MD: US National Institutes of Health. Available at: http://rsb.info.nih/ij/.

[76] Meinhardt G and Hass R (1995). Differential expression of c-*myc*, *max* and *mxi1* in human myeloid leukemia cells during retrodifferentiation and cell death. *Leuk Res* **19** (10), 699–705.

[77] Masters J and Palsson B (1999). Human Cell Culture, Vol. 2: Cancer Cell Lines, Part 2. Kluwer Academic Publishers, Boston, MA, pp. 79–106.

[78] Guppy M, Leedman P, Zu X, and Russell V (2002). Contribution by different fuels and metabolic pathways to the total ATP turnover of proliferating MCF-7 breast cancer cells. *Biochem J* **364** (Pt 1), 309–315.

[79] Langbein S, Zerilli M, Zur Hausen A, Staiger W, Rensch-Boschert K, Lukan N, Popa J, Ternullo MP, Steidler A, Weiss C, et al. (2006). Expression of transketolase TKTL1 predicts colon and urothelial cancer patient survival: Warburg effect reinterpreted. *Br J Cancer* **94** (4), 578–585.

[80] Serkova N and Boros LG (2005). Detection of resistance to imatinib by metabolic profiling: clinical and drug development implications. *Am J Pharmacogenomics* **5** (5), 293–302.

[81] Gillies RJ and Gatenby RA (2007). Adaptive landscapes and emergent phenotypes: why do cancers have high glycolysis? *J Bioenerg Biomembr* **39** (3), 251–257.

[82] Aledo JC (2004). Glutamine breakdown in rapidly dividing cells: waste or investment? *Bioessays* **26** (7), 778–785.

[83] Futcher B, Latter GI, Monardo P, McLaughlin CS, and Garrels JI (1999). A sampling of the yeast proteome. *Mol Cell Biol* **19** (11), 7357–7368.

[84] Khayat ZA, McCall AL, and Klip A (1998). Unique mechanism of GLUT3 glucose transporter regulation by prolonged energy demand: increased protein half-life. *Biochem J* **333** (Pt 3), 713–718.

[85] Benanti JA, Cheung SK, Brady MC, and Toczyski DP (2007). A proteomic screen reveals SCFGrr1 targets that regulate the glycolytic–gluconeogenic switch. *Nat Cell Biol* **9** (10), 1184–1191.

[86] Sears R, Nuckolls F, Haura E, Taya Y, Tamai K, and Nevins JR (2000). Multiple Ras-dependent phosphorylation pathways regulate Myc protein stability. *Genes Dev* **14** (19), 2501–2514.

[87] Yeh E, Cunningham M, Arnold H, Chasse D, Monteith T, Ivaldi G, Hahn WC, Stukenberg PT, Shenolikar S, Uchida T, et al. (2004). A signalling pathway controlling c-Myc degradation that impacts oncogenic transformation of human cells. *Nat Cell Biol* **6** (4), 308–318.

[88] Gao P, Zhang H, Dinavahi R, Li F, Xiang Y, Raman V, Bhujwalla ZM, Felsher DW, Cheng L, Pevsner J, et al. (2007). HIF-dependent antitumorigenic effect of antioxidants *in vivo*. *Cancer Cell* **12** (3), 230–238.

[89] Chun YS, Lee KH, Choi E, Bae SY, Yeo EJ, Huang LE, Kim MS, and Park JW (2003). Phorbol ester stimulates the nonhypoxic induction of a novel hypoxia-inducible factor 1α isoform: implications for tumor promotion. *Cancer Res* **63** (24), 8700–8707.

[90] Zhong H, Hanrahan C, van der Poel H, and Simons JW (2001). Hypoxia-inducible factor 1α and 1β proteins share common signaling pathways in human prostate cancer cells. *Biochem Biophys Res Commun* **284** (2), 352–356.

[91] Marampon F, Ciccarelli C, and Zani BM (2006). Down-regulation of c-Myc following MEK/ERK inhibition halts the expression of malignant phenotype in rhabdomyosarcoma and in non muscle–derived human tumors. *Mol Cancer* **5**, 31.

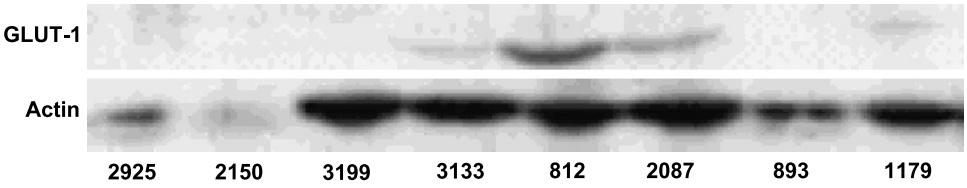

Figure W1. GLUT-1 protein expression. Immunoblot analysis of GLUT-1 and actin from whole–tumor cell lysates.